

## Supplementary information

### Mechanobiological Regulation of T Cells via Transient Viscoelastic Microfluidic Confinement

Mohammad Asghari<sup>1</sup>, Morteza Aramesh<sup>2</sup>, Prerit Mathur<sup>1</sup>, Yingchao Meng<sup>1</sup>, Margherita Bernero<sup>2</sup>, Viola Vogel<sup>3</sup>, Stavros Stavrakis<sup>1\*</sup> and Andrew J. deMello<sup>1\*</sup>

*1. Institute for Chemical and Bioengineering, ETH Zürich, Vladimir Prelog Weg 1, Zürich, 8093, Switzerland.*

*2. Institute for Biomedical Engineering, Department of Information Technology and Electrical Engineering, Gloriastrasse 37/39, ETH Zürich, Zürich, 8092, Switzerland*

*3. Institute of Translational Medicine, Department for Health Sciences and Technology, Gloriastrasse 39, ETH Zürich, Zürich, 8092, Switzerland.*

\* Corresponding authors: [stavros.stavrakis@chem.ethz.ch](mailto:stavros.stavrakis@chem.ethz.ch), [andrew.demello@chem.ethz.ch](mailto:andrew.demello@chem.ethz.ch)

## Supplementary text.

### Computational model of cell deformation

The deformation of cells was analyzed using a fluid–structure interaction (FSI) framework implemented in COMSOL Multiphysics 6.3.

The suspending fluid was treated as incompressible and described by the Navier–Stokes equations:

$$\rho_f \frac{\partial \mathbf{u}}{\partial t} + \rho_f (\mathbf{u} \cdot \nabla) \mathbf{u} = \nabla \cdot [-p\mathbf{I} + \boldsymbol{\kappa}] \quad (1)$$

$$\rho_f \nabla \cdot \mathbf{u} = 0 \quad (2)$$

$$\boldsymbol{\kappa} = \mu_f (\nabla \mathbf{u} + (\nabla \mathbf{u})^T) \quad (3)$$

where  $\rho_f$  is fluid density,  $\mathbf{u}$  is velocity,  $p$  is pressure,  $\mathbf{I}$  is the identity tensor, and  $\mu_f$  is the fluid's dynamic viscosity.

Cells were modeled as nonlinear hyperelastic solids following a neo-Hookean constitutive law:

$$\rho_c \frac{\partial^2 \mathbf{u}_c}{\partial^2 t} = \nabla \cdot (\mathbf{F}\mathbf{S})^T \quad (4)$$

where  $\rho_c$  denotes cell density,  $\mathbf{u}_c$  the displacement vector,  $\mathbf{F}$  the deformation gradient, and  $\mathbf{S}$  the second Piola–Kirchhoff stress.

The strain energy density function  $W_s$  for the neo-Hookean material is given by:

$$W_s = \frac{1}{2} \mu (\bar{\mathbf{I}}_1 - 3) + \frac{1}{2} \kappa (J_{el} - 1)^2 \quad (5)$$

where  $\bar{\mathbf{I}}_1$  is the first invariant of the isochoric deformation tensor,  $J_{el}$  the elastic volume ratio,  $\mu$  the shear modulus, and  $\kappa$  the bulk modulus. For incompressible materials,  $\mu$  and Young's modulus  $E$  are related by  $\mu = E/3$ .

The coupled equations were solved using a Newton iteration scheme for time-dependent nonlinearities and discretized with the finite element method. The linear systems were handled with the PARDISO direct solver. The velocity field (Navier–Stokes) was discretized using linear Lagrange elements, and the cell surface displacement field was likewise discretized with linear elements.

The inlet velocity profile was first calculated without the cell, based on imposed flow rate, channel geometry, and fluid properties. This was then applied as a Dirichlet boundary condition at the channel entrance. Atmospheric pressure was imposed at the outlet to avoid backflow. To ensure the cell remained centered in the computational domain, all quantities were expressed in a moving reference frame following the cell, and the Arbitrary Lagrangian–Eulerian (ALE) method was employed to accommodate fluid-domain deformation.

Cell deformation was quantified using the deformation index  $D$ :

$$D = 1 - \frac{2\sqrt{\pi A}}{l} \quad (6)$$

where  $A$  is the projected cell area and  $l$  is the cell perimeter, both obtained directly from the simulations.

### **Simulation results of velocity, shear stress, and deformation across confinement sizes**

For the simulations, we modeled a T cell with a diameter of  $\sim 6.1 \mu\text{m}$  (the average size of non-activated T cells measured experimentally, Fig. 1d) and assigned a Young's modulus of 0.4 kPa, consistent with reported values for T cells.<sup>1</sup> Simulations were performed for channel heights of 15, 10, and 5  $\mu\text{m}$ , all subjected to the same inlet pressure of 1500 mbar as in the experiments. As shown in Fig. S6a, flow velocity increases with channel height, with maximum values of 0.73, 0.43, and 0.19 m/s for 15, 10, and 5  $\mu\text{m}$  channels, respectively. Fig. S6b shows that the local shear rate fields also peak in the larger channels ( $22 \times 10^4$ ,  $18 \times 10^4$ , and  $13 \times 10^4 \text{ s}^{-1}$  for 15, 10, and 5  $\mu\text{m}$ , respectively). However, these elevated shear-rate regions are located close to the channel walls, where cells do not reside due to viscoelastic focusing (cell boundary shown in red). Instead, cells travel along the channel centerline. When a cell is positioned centrally, the effective shear environment experienced by the cell is greater in the more confined geometries, since the cell cross-section occupies a larger fraction of the channel height.

This interpretation is confirmed by direct calculation of WSS on the cell membrane (Fig.S6c). Despite the lower fluid velocity and shear-rate maxima in the 5  $\mu\text{m}$  height channel, the WSS on the cell surface is highest, because the cell nearly fills the channel and makes contact with the walls. The mean WSS values were 1.30 kPa (5  $\mu\text{m}$  height channel), 0.41 kPa (10  $\mu\text{m}$  height channel), and 0.26 kPa (15  $\mu\text{m}$  height channel). The predicted cell deformation values (0.065,

0.055, and 0.034 for 5, 10, and 15  $\mu\text{m}$  channels, respectively, Fig.S6d) closely matched the experimentally measured averages (0.062, 0.058, and 0.039; Fig. 1d), further validating our model.

Taken together, these results highlight that geometric confinement, rather than bulk velocity or channel-averaged shear rate, is the key factor governing mechanical load on the cell. In wide channels (10–15  $\mu\text{m}$ ), the cell remains suspended away from the walls and experiences relatively uniform shear. In the most confined geometry (5  $\mu\text{m}$ ), however, the cell is compressed against the channel boundaries, producing elevated local shear stresses and greater deformation.

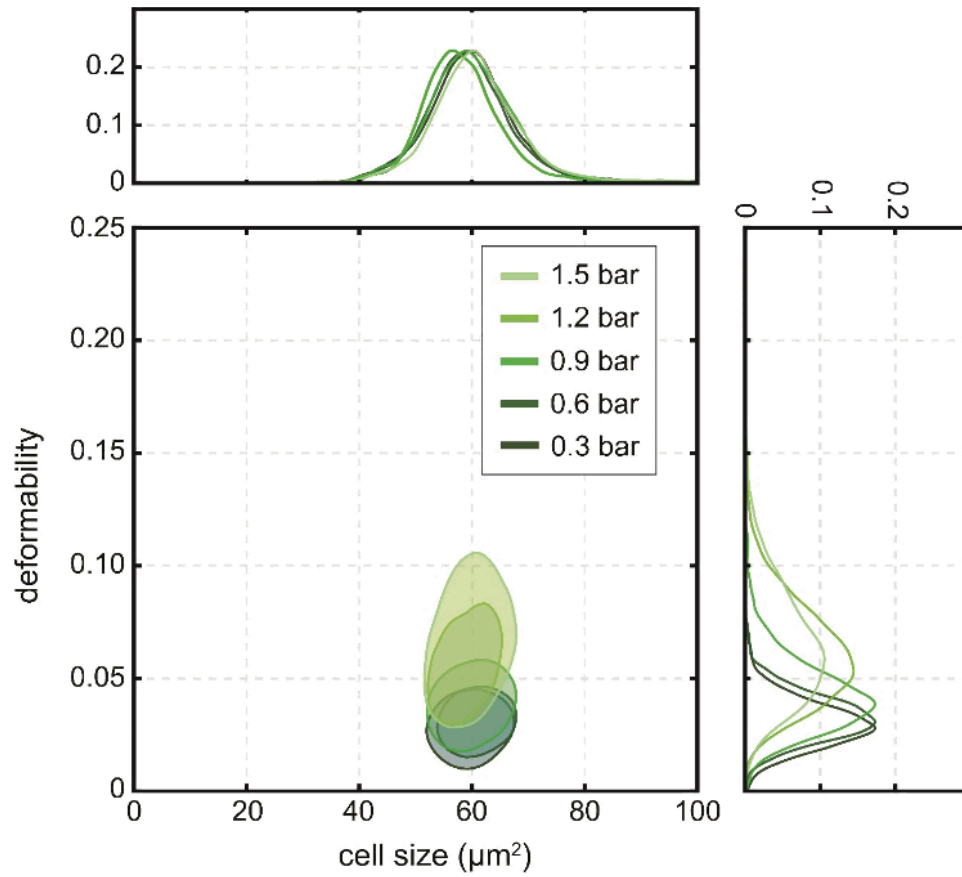


**Figure S1. Analysis of the effects of inlet pressure on activated T cell deformability.** Higher pressures induce higher shear stresses on cells resulting in an upward shift in cell deformability with cell size remaining essentially constant.

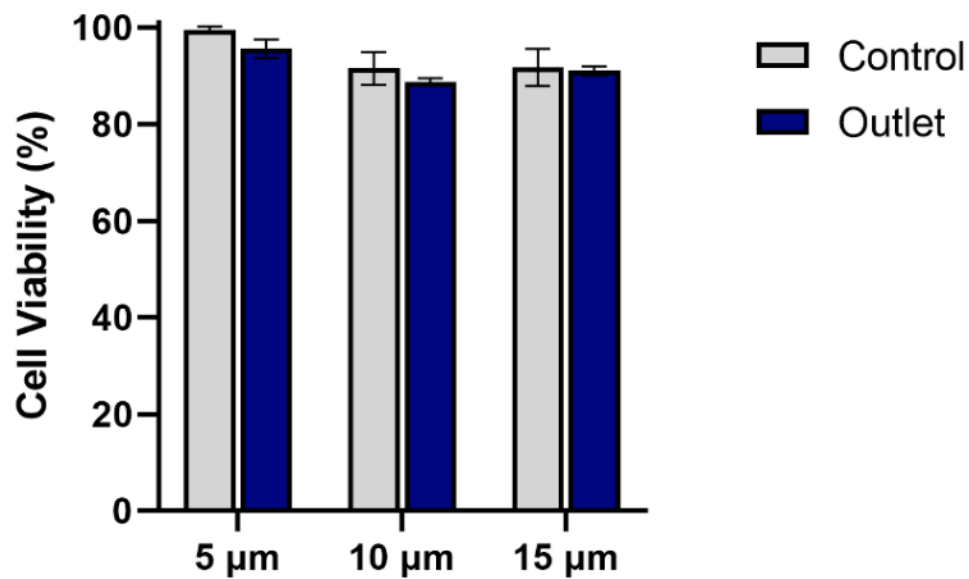


**Figure S2. Viability of T cells 4 hours after confinement in microchannels of variable height using a Zombie NIR fixable viability test.** Processing through all tested channels resulted in high viabilities (>85%), with no significant difference compared to the inlet sample (control).

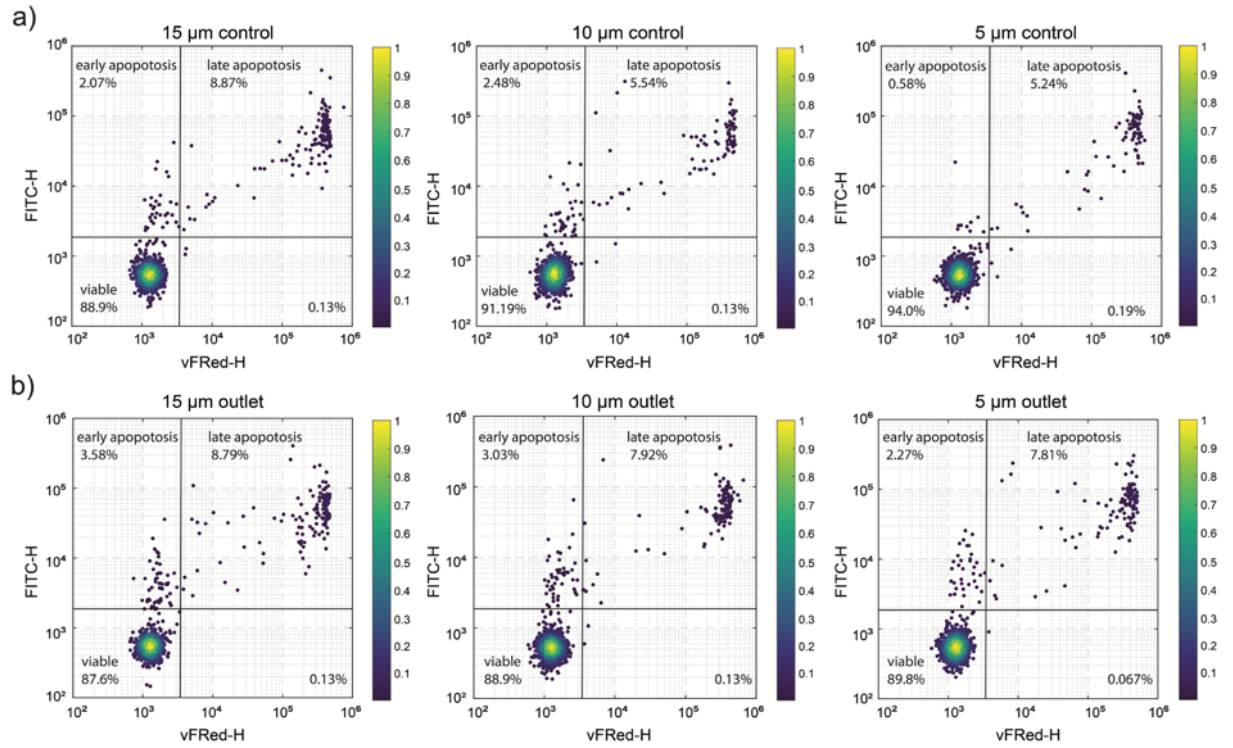


**Figure S3. Apoptosis analysis of T cells by flow cytometry.** (a) 4 hours before confinement and (b) 4 hours after confinement using different microfluidic geometries (15  $\mu$ m, 10  $\mu$ m and 5  $\mu$ m high from left to right). Confinement experiments show a very small decrease in the percentage of viable cells after confinement.

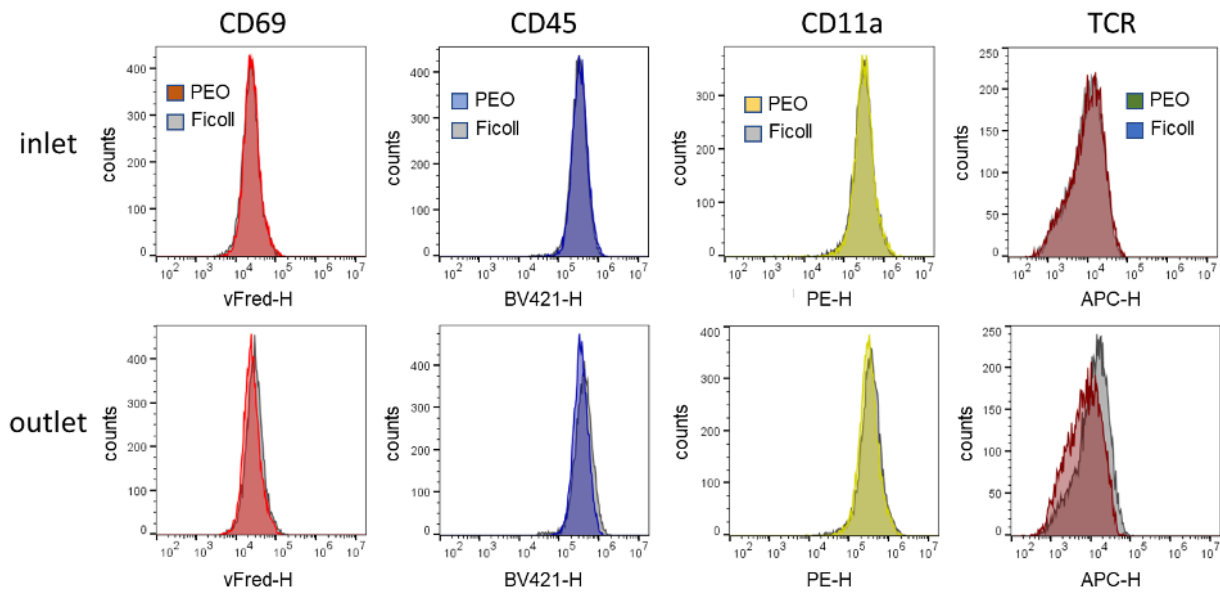


**Figure S4. Protein expression for T cells in PEO and Ficoll density gradient medium.** No significant differences in protein expression were observed for T cells in either PEO or Ficoll density gradient medium at the inlet and at the outlet of 15  $\mu$ m high microfluidic channels.



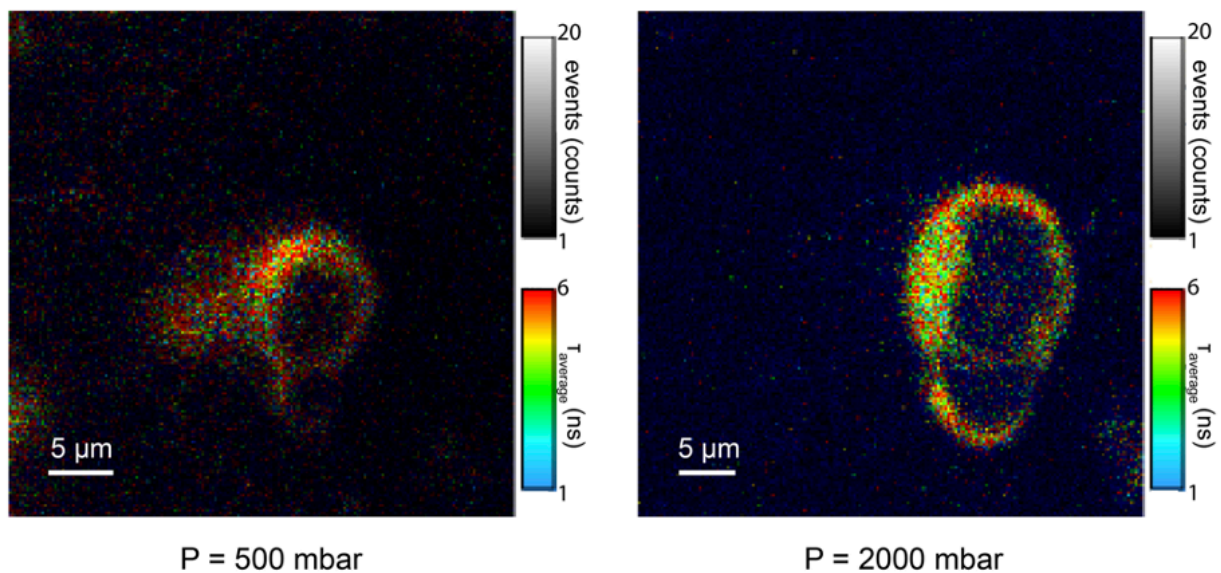


**Figure S5. FLIM images of a cell being compressed using a PDMS pneumatic valve.** Different compressive stress conditions trigger distinct cell responses, observable through changes in the average fluorescence lifetime.

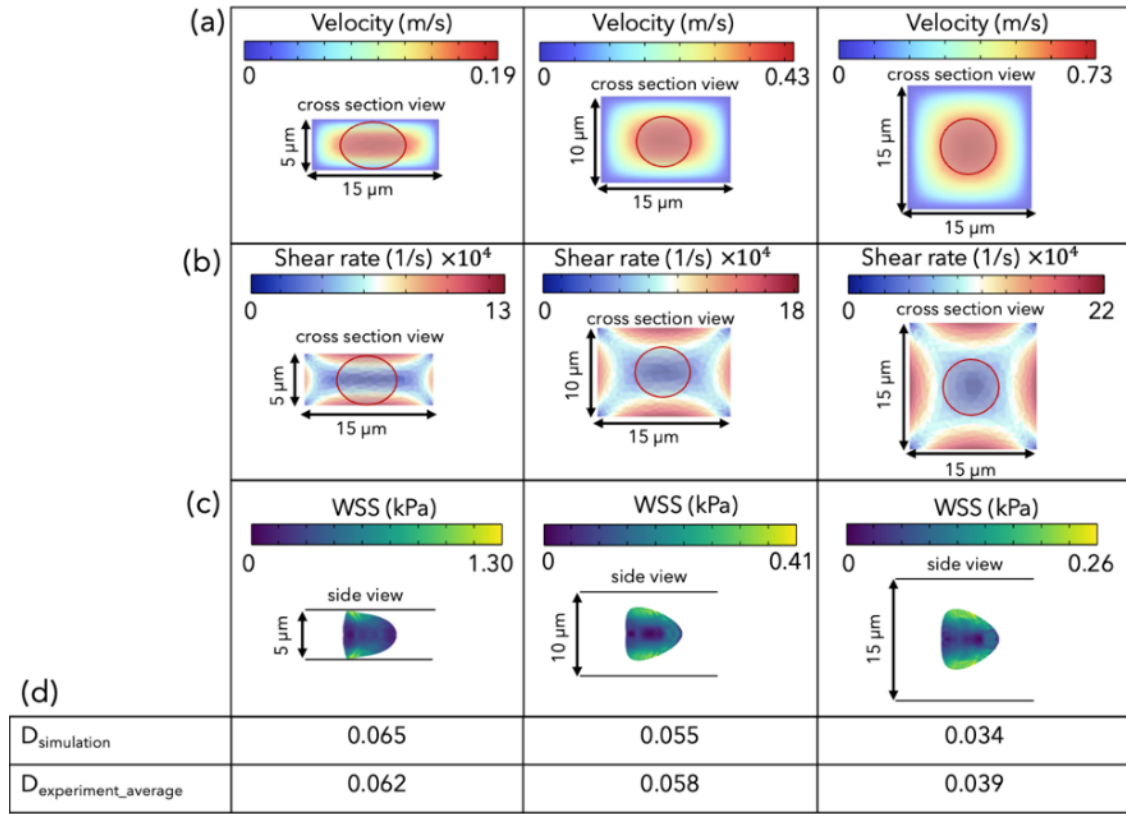


**Figure S6. Numerical simulations of velocity, shear rate, wall shear stress, and cell deformation in microchannels of varying confinement.** (a) Velocity profiles in 5, 10, and 15  $\mu\text{m}$ -high channels at an inlet pressure of 1500 mbar. Maximum velocities were 0.19, 0.43, and 0.73 m/s, respectively. (b) Local shear-rate distributions in the same channels. Although the peak shear rates are highest in the larger channels ( $22 \times 10^4$ ,  $18 \times 10^4$ , and  $13 \times 10^4 \text{ s}^{-1}$  for 15, 10, and 5  $\mu\text{m}$ ), these maxima occur near the channel walls. Cells (shown as red boundaries, average diameter 6.1  $\mu\text{m}$ ) travel along the channel centerline due to viscoelastic focusing, so the effective shear environment increases with confinement as cells occupy a larger fraction of the channel height and wall region. (c) Wall shear stress (WSS) on the cell membrane. Despite lower bulk velocity and shear-rate maxima in the 5  $\mu\text{m}$  channel, the WSS on the cell surface is highest under this condition (1.30 kPa), compared to 0.41 kPa and 0.26 kPa in the 10 and 15  $\mu\text{m}$  channels, respectively. This results from direct contact between the cell and the channel walls in the most confined geometry. (d) Comparison of deformation indices from simulations and experiments shows strong agreement: 0.065 vs. 0.062 (5  $\mu\text{m}$ ), 0.055 vs. 0.058 (10  $\mu\text{m}$ ), and 0.034 vs. 0.039 (15  $\mu\text{m}$ ).

## References

- 1 B. Fregin, F. Czerwinski, D. Biedenweg, S. Girardo, S. Gross, K. Aurich and O. Otto, *Nat. Commun.*, 2019, **10**, 415.